Electronic band structure of semiconductor nanostructure arrays

Garnett W. Bryant
McDonnell Douglas Research Laboratories, St. Louis, Missouri 63166-0516
(Received 28 September 1988; revised manuscript received 21 February 1989)

Layered, semiconductor superlattices with well widths comparable to the electron wavelength are routinely grown to tailor the electronic properties of artificially structured materials. With the recent advances in the art of nanofabrication, two-dimensional arrays of quantum nanostructures, which should exhibit three-dimensional, quantum, carrier confinement, can be made. Quantum-nanostructure arrays constitute a new generation of artificially structured materials with tailorable electronic properties. In a superlattice, zone folding of the band structure occurs only for bands along the growth direction. However, for a two-dimensional array of nanostructures, the zone folding can be tailored in two directions allowing more band mixing and the possibility of greater band alteration. We have performed augmented-plane-wave calculations for independent electrons in a two-dimensional array of two-dimensional, circular, quantum nanostructures to explore the possibilities of tailoring a two-dimensional band structure. Band structures are presented for arrays formed from different types of nanostructures: quantum boxes (wells), quantum bumps (barriers), and quantum resonators (a well surrounded by a thin barrier to allow resonant trapping in the well). Low-energy band states are quasibound in quantum-box arrays. The low-energy states channel between bumps in quantum-bump arrays. In quantum-resonator arrays, the low-energy states can be channeling states or resonant states. Useful electronic properties that can be controllably tailored are identified and discussed.

I. INTRODUCTION

The energy levels of electrons in a quantum well are modified by the confinement when the well width is comparable to or smaller than the electron wavelength. Layered superlattices of semiconductor quantum wells are now routinely grown to tailor the electronic properties of artificially structured materials. Band gaps and effective masses can be altered by varying layer compositions and thicknesses.

In a superlattice, a one-dimensional, periodic potential (the variation in composition) modifies the band structure of a three-dimensional material. By use of current nanofabrication techniques a one-dimensional periodic potential or patterning can be imposed on a two-dimensional layer,[1] creating an array of quantum wires, and a two-dimensional periodic potential or patterning can be imposed on a two-dimensional layer,[2,3] creating an array of quantum boxes. In this paper we will explore theoretically the possibilities of tailoring the electronic properties of a two-dimensional layer by use of an imposed, two-dimensional, periodic array of potentials or patterning.

Others have previously suggested that two-dimensional device arrays could be used to modify electronic properties and have calculated the band structure and collective excitations for the arrays.[4–10] Our aim in this paper[10] is to explore how the band structure of a two-dimensional layer can be modified by arrays of different types of quantum nanostructures: quantum boxes (wells), quantum bumps (barriers), and quantum resonators (a well surrounded by a thin barrier to allow resonant trapping in the well).

In the next section we will present the motivation for this work, the model used, and the approach taken to calculate band structures. Band structures for two-dimensional layers modified by a two-dimensional periodic potential are presented in Sec. III. Charge densities of selected electronic states are presented to illustrate the character of states in the arrays. Conclusions are discussed in the last section.

II. MODEL, MOTIVATION, AND METHOD

In this paper, two-dimensional arrays, with lattice constants A_x and A_y, of two-dimensional, circular quantum nanostructures (see Fig. 1) are modeled. We assume that the third dimension is a narrow well with only one occupied subband, as is typical for quasi-two-dimensional systems, and can be ignored. We consider conduction electrons. The effective-mass approximation, with an isotropic mass, is used to describe motion in the layer in the absence of the imposed array of potentials.

We assume that the array of nanostructures is defined by a two-dimensional, periodic variation in the composition of the layer. The heterojunctions between well and barrier materials determine the boundaries of the nanostructures. The nanostructure potential is determined by the conduction-band offsets of the materials which are the well and barrier regions. Arrays made from three different structures have been considered (see Fig. 2). Quantum boxes are finite well regions surrounded by connected barrier regions. Quantum bumps are finite barrier regions surrounded by connected well regions. Quantum resonators (or "doughnuts") are finite well regions sur-

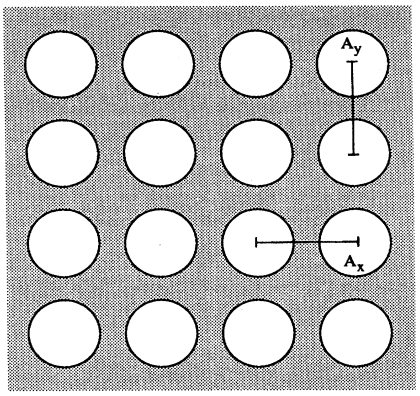

FIG. 1. Two-dimensional array, with lattice constants A_x and A_y, of two-dimensional, circular nanostructures.

rounded by barriers with finite thickness which are surrounded by connected well regions.

For simplicity, we assume that the heterojunction potential profiles are abrupt, as shown in Fig. 2. No attempt has been made to account for charge depletion or accumulation at the interfaces or to include a compositional grading at the interfaces. Arrays made with nanostructures that have abrupt interfaces have not yet been fabricated. However, arrays of nanostructures with graded interfaces have been made by use of ion implanting and annealing to enhance interdiffusion in the patterned regions of a well (Cibert *et al.*[3] and Petroff *et al.*[3]). Arrays have also been made by modulating a two-dimensional layer with a two-dimensional periodic gate potential (Bernstein and Ferry[3]) and with a patterned strain in the barrier layer adjoining the well (Kash *et al.*[3]). These potentials do not have abrupt profiles either. The calculations we perform could be done with graded interfaces. We leave that for future consideration. Although our model assumes that the potential profile is determined by heterojunction band offsets, only the potential profile is used in the calculation. In our model we also include the effects of any well-barrier effective-mass discontinuity. However the effects of this discontinuity are small for most well-barrier systems. Thus, the band structures for arrays defined by gates or patterned strain should be qualitatively the same as the band structures we calculate for nanostructures defined by heterojunctions, provided that the potential profiles are similar.

The effects of a two-dimensionally periodic potential on a two-dimensional layer differ from the effects of a one-dimensional, periodic potential, as in a superlattice, in two important respects. When a periodicity is imposed, zone folding of the band structure occurs. The zone-folded band structure for a free electron in a two-dimensional layer with imposed period (but no potential) $A_x = A_y = 30$ nm is shown in Fig. 3. In a one-

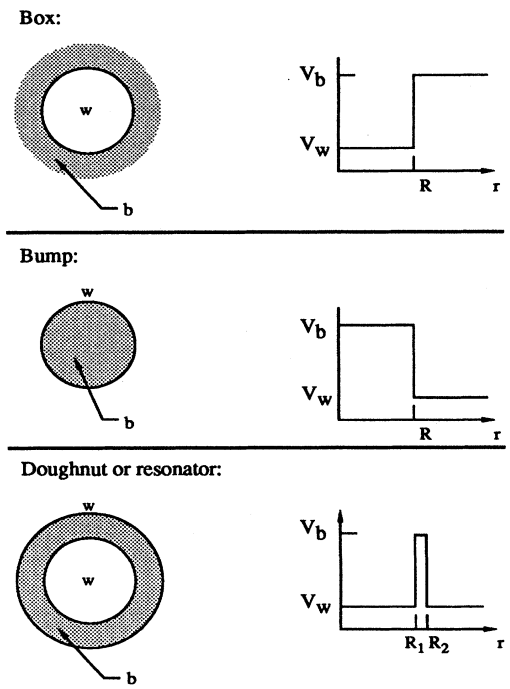

FIG. 2. Configuration and radial potential, as determined by the conduction-band offsets, for quantum-box, quantum-bump, and quantum-resonator nanostructures. Well and barrier regions are denoted w and b. The band edges for well and barrier are V_w and V_b. R is the radial dimension of the structure.

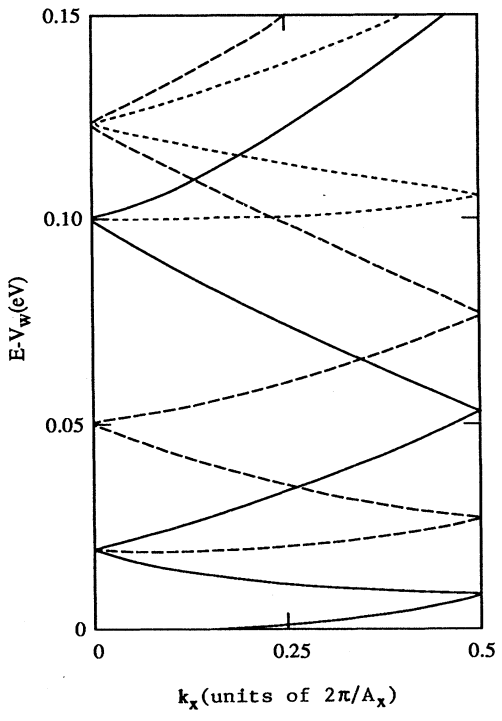

FIG. 3. Zone-folded, two-dimensional, free-electron band structure. The lattice constants are $A_x = A_y = 30$ nm. k_x dispersion for $k_y = 0$ (solid curves), $k_y = \pm 2\pi / A_y$ (dashed curves), and $k_y = \pm 4\pi / A_y$ (dotted curves) are shown. The electron effective mass is $m = 0.067 m_e$.

dimensional superlattice, zone folding occurs only in one direction, and only the $k_y=0$ band in Fig. 3 is present. When a two-dimensional periodicity is imposed, additional doubly degenerate zone-folded bands appear for $k_y=\pm 2\pi n/A_y$ with $n=1,2,3,\ldots$. These new bands are replicas of the $k_y=0$ band shifted to higher energy by $E(k_x=0,\ k_y=2\pi n/A_y)$. There is much greater opportunity for band modification when a two-dimensional periodicity is imposed because a single band can have multiple crossings with its zone-folded replicas. Of course, a band can also have crossings with other types of bands. Here we are considering the case where different types of bands (s and p bands, for example) are widely separated in energy. Zone folding and crossing of replica bands occur in a bulk crystal on an eV energy scale because $A_x \lesssim 1$ nm. In two-dimensional nanostructure arrays, $A_x \sim 10$ nm and the zone folding and band crossings occur on a meV energy scale, which is the energy scale that is relevant for electronic states important in device applications.

When a two-dimensional array of nanostructures is used to tailor electronic properties, the choice of nanostructure—box, bump, resonator—provides a degree of freedom to tailor the electronic states which is not available with a superlattice of barriers and wells. Quantum boxes could be used to localize electrons in finite regions. Quantum bumps could be used to define channels, which in turn could be connected to form a network. Quantum resonators could be constructed so that states trapped resonantly within the resonator would overlap in energy and hybridize with extended states which channel between resonators. One aim of this paper is to determine (1) whether quantum boxes in an array can still localize states effectively, (2) whether quantum bumps can define channels, and (3) whether quantum resonators can be designed to hybridize quasilocalized and extended states.

To answer these questions we have performed augmented-plane-wave (APW) calculations[11] for the band structure of two-dimensional electrons moving in the periodic potential defined by the nanostructure array. The modification of the three-dimensional APW method[11] to do a two-dimensional APW calculation is straightforward. The APW calculations are done for independent electrons; no attempt is made to include depletion profiles. The APW method requires that the Schrödinger equation be solved in a central core out to the muffin-tin radius. In our case, this core region includes the nanostructure and a finite circular annulus of the region surrounding the nanostructure. Since the potential is piecewise constant in the core, solutions to the Schrödinger equations are Bessel functions in each region of the potential. By matching solutions as each interface in the nanostructure and accounting for the mass discontinuity at each interface, the wave function at the edge of the core can be determined. A more complicated potential would require a numerical solution of the Schrödinger equation.

Band structures for different nanostructures and arrays can be related by the following scaling argument. If distances are scaled by a factor λ (prime and unprimed quantities for scaled and original structures)

$$A_x'=\lambda A_x,\quad A_y'=\lambda A_y,\quad R_i'=\lambda R_i\ ,$$

where the R_i (see Fig. 2) are the radial dimensions which define the nanostructure and the band offsets are scaled as

$$V_b'-V_w'=(V_b-V_w)/\lambda^2$$

[V_b (V_b') and V_w (V_w') are the barrier and well band edges in the original (scaled) structure], then the energies E and E' of equivalent states in the original and scaled systems are related by

$$E'-V_w'=(E-V_w)/\lambda^2\ ,$$

provided that differences in the effective masses between the original and scaled structures are small. Thus, different structures will have the same band structure (except for the scale factor $1/\lambda^2$) if other energies and potentials scale as $1/\lambda^2$ and distances scale as λ.

III. ARRAY BAND STRUCTURES

We have calculated the band structures for quantum-box, quantum-bump, and quantum-resonator square arrays to show how electronic states of a two-dimensional layer can be modified by different nanostructure arrays. We present results for square arrays with $A_x=A_y=30$ nm. To present results which are typical for semiconductor structures, we use the following material parameters: The effective mass in the wells is $m_w=0.067m_e$, and the barrier material is an alloy, x is the deviation of the alloy composition from the well material, with $m_b=m_w+0.083xm_e$ and $V_b=V_w+(0.74\text{ eV})x$. We present band structures as a function of x to show how variations in barrier height change the electronic states. For quantum-box and -bump arrays the band structures are presented for nanostructures with fixed size ($R=8$ nm) as a function of barrier composition ($x=0.05$, 0.1, and 0.2). Band structures are presented for quantum-resonator arrays, with fixed composition and outer radius ($x=0.4$, $R_2=13$ nm), as a function of inner-hole radius ($R_1=6$, 9, 11 nm). When $x=0$, all three arrays produce the same band structure—the zone-fold free-electron band structure shown in Fig. 3. Only the band structure in the x direction is shown in the figures. Bands in other directions have been calculated and are similar. The charge densities of selected states are presented to illustrate the character of those states. Dipole matrix elements for valence- to conduction-band transitions are also presented for selected states to illustrate their character.

A. Quantum-box arrays

The band structure for a quantum-box array with $x=0.05$ (Fig. 4) is similar to the zone-folded, free-electron band structure. The corresponding bands are easy to identify. However, band mixing, avoided crossings, and distortion are also evident when $x=0.05$. Band gaps are present at the zone edges. One quasibound state

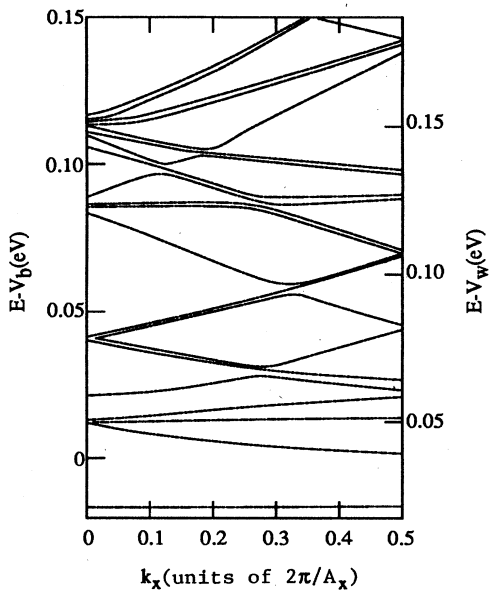

FIG. 4. Band structure in the x direction for a quantum-box array: $A_x = A_y = 30$ nm, $R = 8$ nm, $x = 0.05$, and $V_b - V_w = 0.037$ eV.

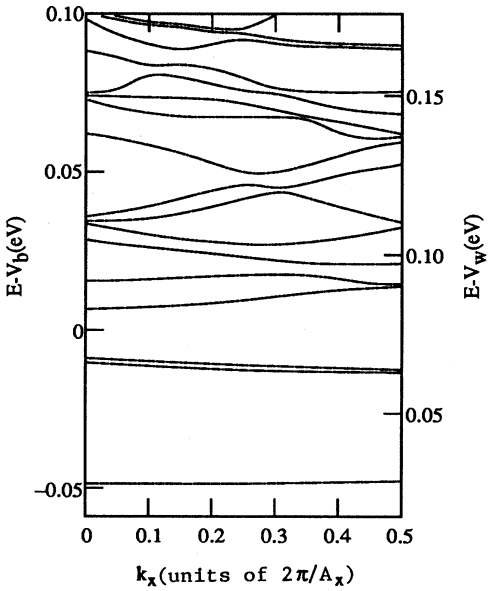

FIG. 5. Band structure for a quantum-box array: Same as Fig. 4 except that $x = 0.1$ and $V_b - V_w = 0.074$ eV.

exists and the doubly degenerate free-electron bands for $k_y = \pm 2\pi n / A_y$ are split. As x increases (Figs. 5 and 6), substantial band distortion occurs and the correspondence with zone-folded free-electron bands is difficult to identify.

The ordering of the bands changes as x increases. For example, when $x = 0.05$, the third and fourth bands are close in energy. When $x = 0.1$, the second and third bands are quasidegenerate, and the fourth band is pushed to higher energy by level repulsion. This reordering is necessary to provide the correct degeneracies for quasi-bound states. The ground state in an isolated circular box is nondegenerate. Other bound states are doubly degenerate. Three quasibound states (with the correct degeneracies) appear in the array band structure when $x = 0.1$. Six states are bound when $x = 0.2$. The highest bound state still has dispersion and is not yet doubly degenerate. The dispersion of higher-energy states also decreases as x increases. A comparison of Figs. 4–6 shows that these states are merging into quasi-doubly-degenerate flat bands as x increases. For an array with the same lattice constants but made from larger boxes, more states are quasibound; however, the states have larger energy dispersion because tunneling between boxes is more likely. For example, for boxes with $R = 12$ nm and $x = 0.2$, ten states are quasibound.

The charge density of the lowest-energy zone-center state in the $x = 0.05$ box array is shown in Fig. 7. The quasibound state has an s-like charge density in a box. When the barrier height is increased (see Fig. 8 for states in the $x = 0.2$ array), the s-like lowest-energy, quasibound state is more localized in the box and higher-energy quasibound states also have definite local atomic character (a p-like state is shown in Fig. 8).

As in superlattices, band masses, widths, and gaps can be tailored. For example, the band mass at $k_x = 0$ for the lowest band in Figs. 4–6 increases by factors of 4, 5, and 10 as x increases from 0.01 to 0.05 to 0.1 to 0.2. The band width of the lowest band decreases by similar factors as x increases. The band gap between the two lowest bands increases from 0 to 46 meV as x changes from 0 to 0.2.

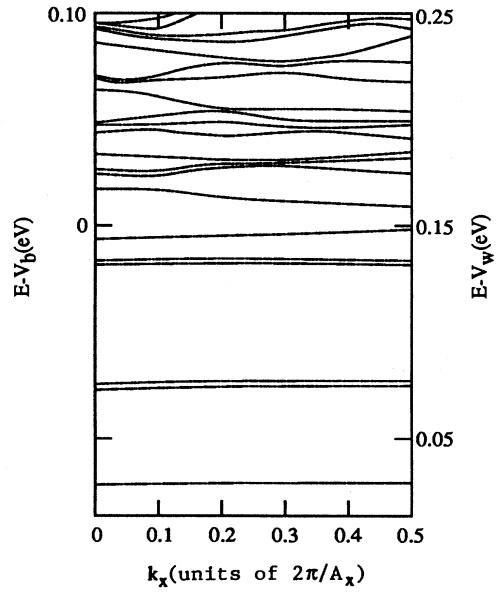

FIG. 6. Band structure for a quantum-box array: Same as Fig. 4 except that $x = 0.2$ and $V_b - V_w = 0.148$ eV.

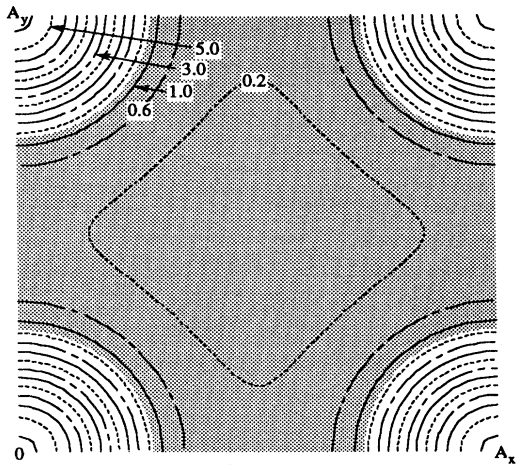

FIG. 7. Charge density of the lowest-energy zone-center ($k=0$) conduction-band state in a quantum-box array with $x=0.05$. One unit cell is shown. The barrier region is shaded. The state is normalized such that a plane wave has unit charge density everywhere.

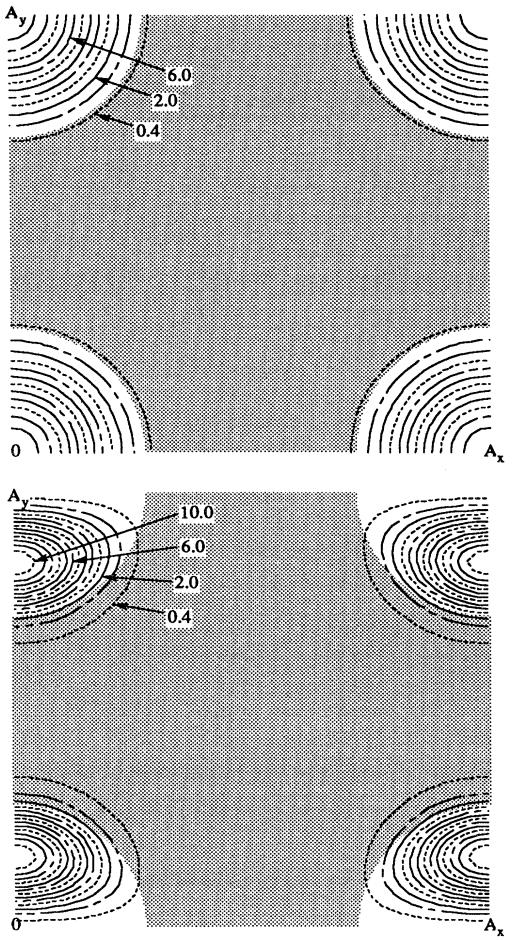

FIG. 8. Charge density of the lowest-energy (top) and first excited (bottom) zone-center conduction states in a quantum-box array with $x=0.2$.

B. Quantum-bump arrays

Band structures for quantum-bump arrays with $x=0.05$, 0.1, and 0.2 are shown in Figs. 9–11. The band structures for quantum-bump and -box arrays are qualitatively different, have different band splittings, orderings, and band gaps. Most importantly, bands in quantum-bump arrays do not lose their dispersion as x increases. In fact, the low-energy bands become independent of x as x increases. For example, the lowest five bands change little as x increases from 0.1 to 0.2. This indicates that these low-energy states do not tunnel into the bump regions and are insensitive to the barrier height. Instead, these states are located in the channels between the bumps. The states are analogous to bonding states in crystals.

The charge densities of the two lowest-energy zone-center states in an $x=0.2$ bump array are shown in Fig. 12. The lowest-energy state is s-like in the central region of well material that is surrounded by four bumps. Substantial charge also exists in the channels that connect adjacent central-well regions. The charge in the first excited state is located in the bonds that connect adjacent central well regions. Figure 13 shows that states at the zone edge ($k_x=\pi/A_x$, $k_y=0$) move along weakly coupled channels in the x direction.

For an array with larger bumps (larger R), the channels are narrower and the coupling between central-well regions is weaker. In this case the low-energy states have less dispersion and are separated by larger gaps. Thus

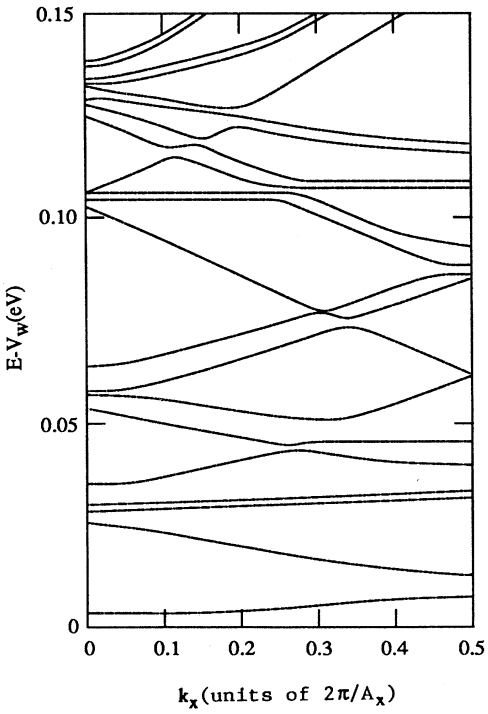

FIG. 9. Band structure for a quantum-bump array: Same as Fig. 4 except that $x=0.05$ in the bump.

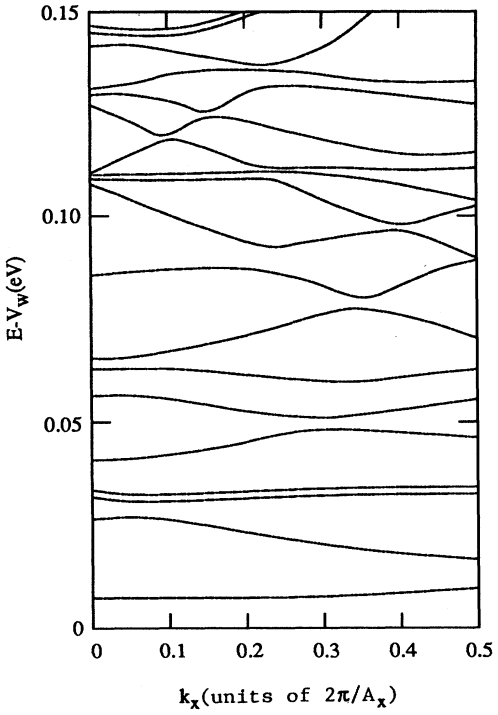

FIG. 10. Band structure for a quantum-bump array: Same as Fig. 9 except that $x=0.1$.

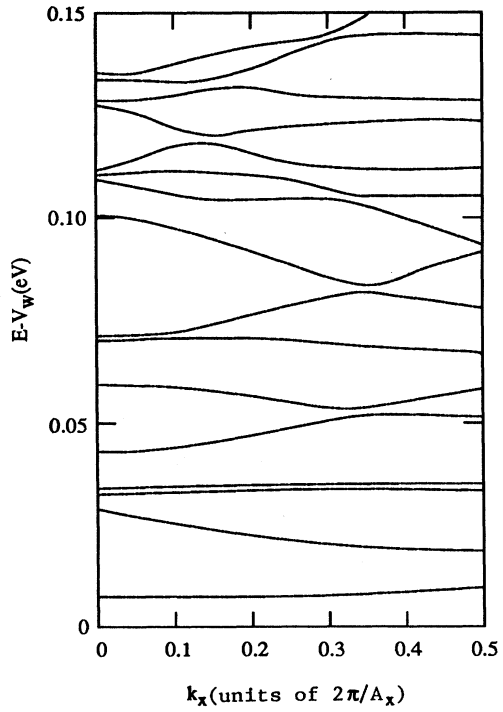

FIG. 11. Band structure for a quantum-bump array: Same as Fig. 9 except that $x=0.2$.

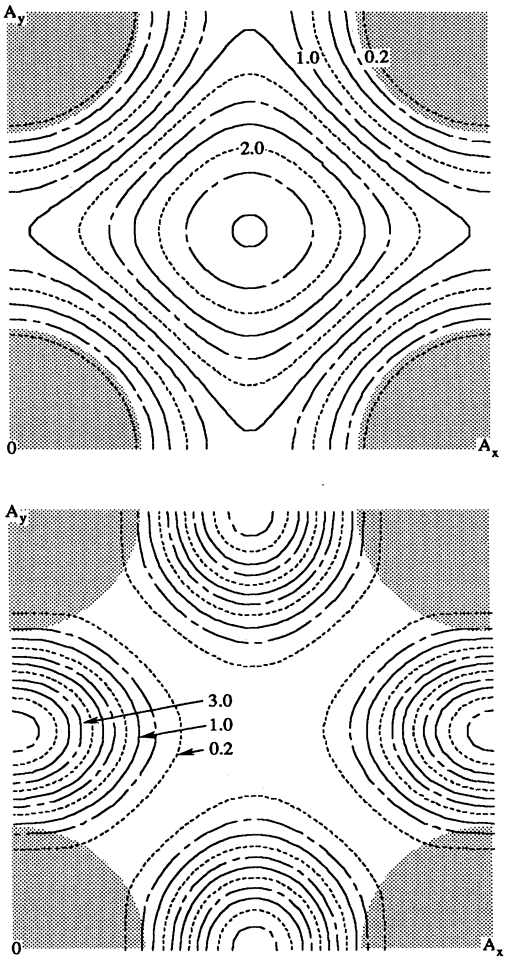

FIG. 12. Charge density of the lowest-energy (top) and first excited (bottom) zone-center conduction states in a quantum-bump array with $x=0.2$.

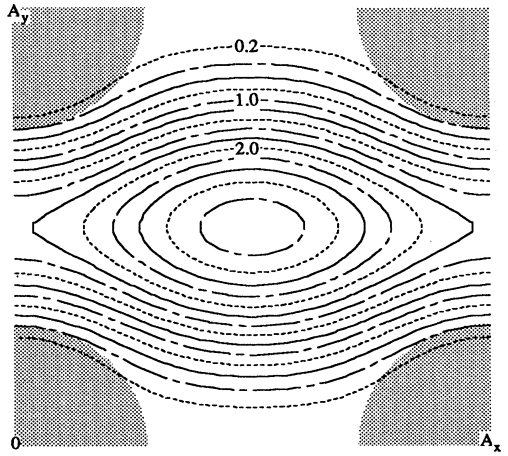

FIG. 13. Charge density of the lowest-energy zone-edge ($k_x=\pi/A_x$, $k_y=0$) conduction state in a quantum-bump array with $x=0.2$.

the strength of the coupling between central-well regions can be controlled by the size of the bumps. When the bumps touch and the central-well regions are decoupled, the array becomes a quantum-box array and the low-energy bands become flat.

C. Quantum-resonator arrays

The low-energy states of quantum-resonator arrays are shown in Figs. 14–16 for resonators ($x=0.4$, $R_2=13$ nm) with different inner cores ($R_1=6$, 9, and 11 nm). Higher-energy states have not been plotted because the band distortions are severe and ordering of high-energy bands is difficult to identify consistently.

Two types of low-energy bands are present. The bands insensitive to R_1 are channeling states, as in quantum-bump arrays, which propagate in the connected well regions but do not tunnel into the cores of the quantum resonator. These states have little dispersion because the channels are narrow ($R_2=13$ nm). The bands which are sensitive to R_1 are resonance states which can tunnel into the resonator core. The ordering and character of the lowest states is shown in Fig. 17. For resonators with large inner cores ($R_1=9$ nm), the lowest-energy state tunnels into the core and the first excited state is a channeling state. For $R_1 \lesssim 9$ nm, the energy of localization in the core is large and the resonance state is the first excited state. For $R_1 \approx 9.5$ nm, the resonance state and channel state are nearly degenerate. A crossover and hybridization of levels occur.

The charge densities for the zone-center, lowest-energy channeling and resonance states are shown in Figs. 18 and 19 for $R_1=9$ and 11 nm, respectively. The trapping of the resonant state in the resonator core is clear. Leakage of the resonance state out of the core and of the channeling state into the core increases as the barrier thickness decreases. When the channeling and resonance states are nearly degenerate ($R_1 \approx 9.5$ nm) the two states

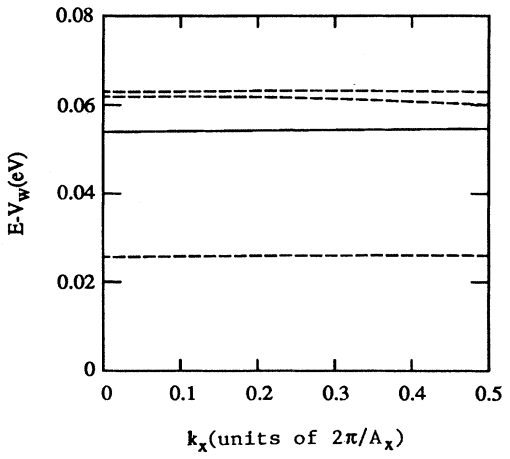

FIG. 14. Band structure for a quantum-resonator array: $A_x=A_y=30$ nm, $R_1=6$ nm, $x=0.4$, and $V_b-V_w=0.296$ eV. Bands of channeling states are shown as dashed curves and bands of resonant states are shown as solid curves.

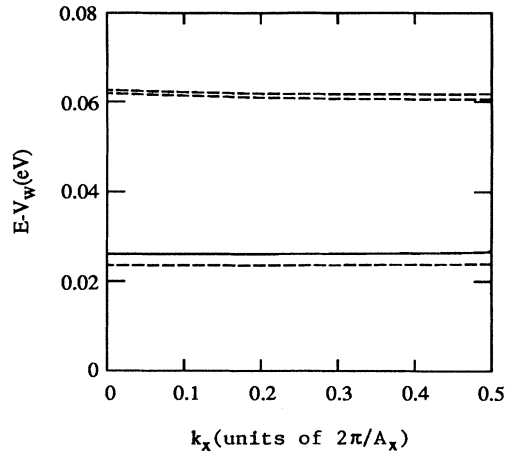

FIG. 15. Band structure for a quantum-resonator array: Same as Fig. 14 except that $R_1=9$ nm.

are strongly hybridized and have nearly the same charge densities. For each state, the charge density inside the resonator core has a magnitude similar to the charge density in the well region outside the resonator, indicating an equal mixing of channeling and resonant character in the strongly hybridized states.

Hybridization and dispersion of channeling states and resonance states can be controlled by the choice of resonator. The resonance level can be varied without affecting the channeling states by keeping R_2 fixed and varying R_1. If R_1 is held fixed and R_2 is varied, the channeling-state dispersion is modified while the resonance state does not change much. The resonance state becomes sensitive to changes in R_2 when $R_1 \approx R_2$ and the states must evolve to the free-electron states. By fixing R_1 and R_2 and increasing the lattice constants, the dispersion of both types of states can be increased.

We obtain additional characterization of the electronic states in a nanostructure array by calculating the dipole matrix elements for transitions between valence and con-

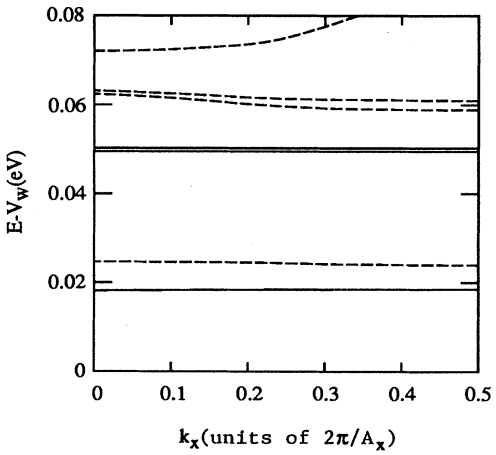

FIG. 16. Band structure for a quantum-resonator array: Same as Fig. 14 except that $R_1=11$ nm.

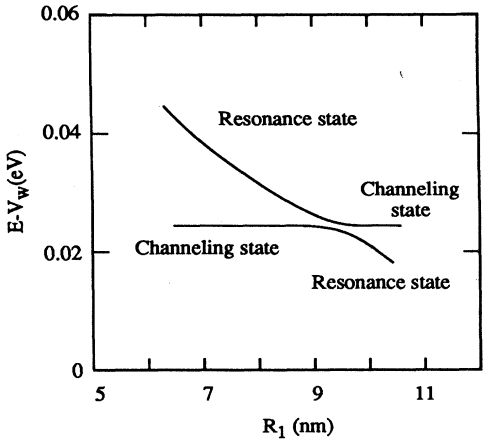

FIG. 17. Lowest-energy resonance and channeling states in a quantum-resonator array as a function of the radius R_1 of the resonator core. A_x, A_y, R_2, and x are the same as in Fig. 14.

duction states with the same wave vector. The dipole matrix elements are proportional to the overlap integrals between the valence and conduction state wave functions in a unit cell of the array (the proportionality constant includes the atomic cell dipole matrix elements). To calculate the overlap integrals, we assume that the valence states are weakly perturbed by the array potential and can be approximated as plane-wave states. In specific cases the overlap integrals would be enhanced or reduced depending on whether or not the nanostructures localize conduction and valence states in the same regions.

When the nanostructure potential is weak and the conduction-band states also are plane waves, the overlap integral vanishes unless the conduction and valence states are in the same band and have the same wave vector. In that case, the integral is unity. When the array potential is present, the overlap between conduction and valence states in the same band is reduced and the overlap be-

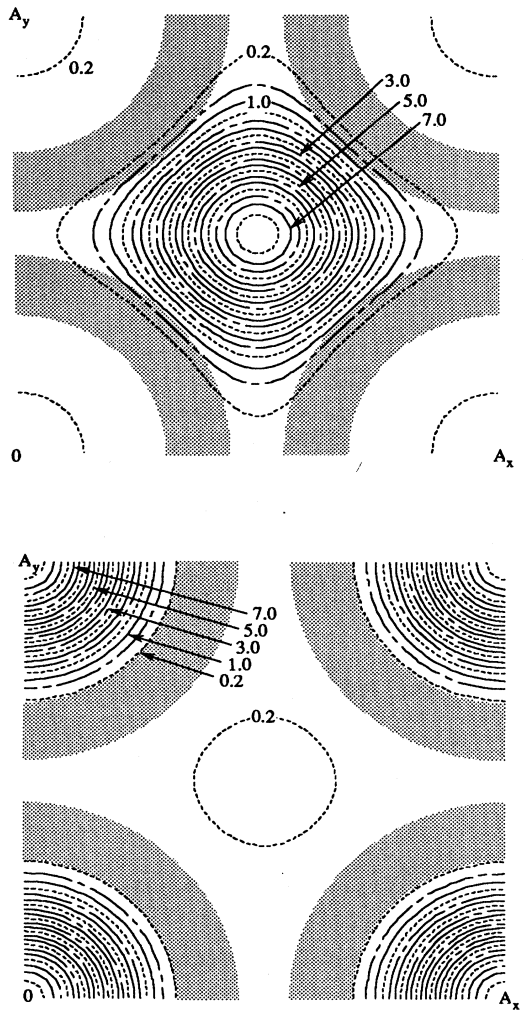

FIG. 18. The charge density for the lowest-energy (top) and first excited (bottom) zone-center states in a quantum-resonator array with $R_1=9$ nm. The states are channeling and resonant states, respectively.

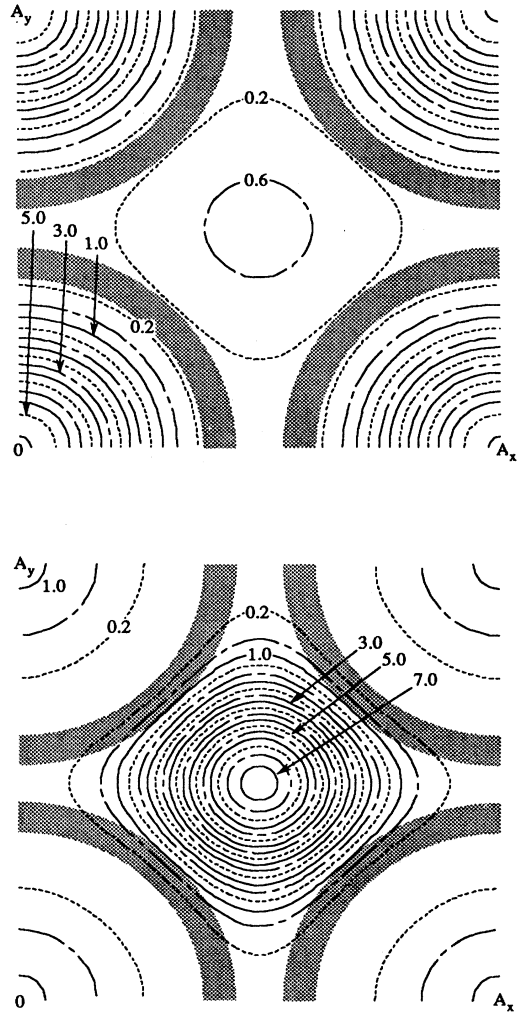

FIG. 19. The charge density for the lowest-energy (top) and first excited (bottom) zone-center states in a quantum-resonator array with core radius $R_1=11$ nm. The states are resonant and channeling states, respectively.

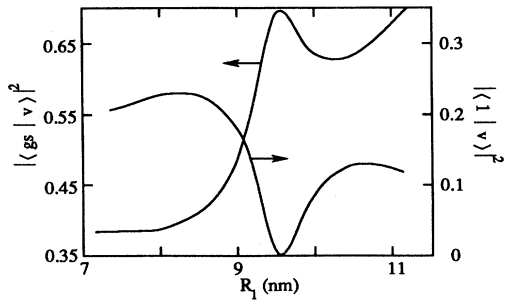

FIG. 20. Overlap matrix elements between a zone-center plane-wave valence state and the lowest-energy (first excited) zone-center conduction states (denoted $\langle gs|v\rangle$ and $\langle 1|v\rangle$, respectively) in a quantum-resonator array as a function of core radius R_1.

tween states in different bands becomes finite.

The overlap integral for the transition between a zone-center valence state in the lowest-energy hole band (first Brillouin zone) and the lowest energy zone-center conduction state is approximately the fraction of the array unit cell occupied by the conduction state. For quantum-box (quantum-bump) arrays with well-localized zone-center ground states, the overlap integrals are approximately the fraction of the array unit cell occupied by the box (region between bumps).

The hybridization of states in a quantum-resonator array has a clear effect on the overlap integrals and dipole matrix elements. Figure 20 shows the overlap integrals between the zone-center valence state and the two lowest-energy conduction states in quantum-resonator arrays as a function R_1. For small R_1, each overlap integral increases as R_1 increases because each state occupies more of the array unit cell when the barrier is thinner. When the channeling and resonant states are nearly degenerate and strongly hybridize ($R_1 \approx 9.5$ nm) the overlap of the valence state to the lowest-energy conduction state peaks and the overlap to the first excited state nearly vanishes. Both conduction states are nearly equal mixtures of channeling and resonant states. The mixing is in phase for the ground state, and so the ground state strongly overlaps the valence plane-wave state. The mixing is out of phase for the excited state and that state is orthogonal to the plane wave. For $R_1 > 9.5$ nm, the hybridization weakens and both overlaps are finite. When $R_1 \approx R_2$, the barrier is a weak perturbation and the conduction states are plane waves. Thus the overlap to the ground state (first excited state) approaches unity (vanishes) when $R_1 \approx R_2$.

IV. CONCLUSIONS

Augmented-plane-wave band-structure calculations have been performed to determine whether a two-dimensionally periodic potential can be used to effectively tailor the electronic properties of a two-dimensional layer. When a two-dimensionally periodic potential is imposed, zone folding of the band structure occurs in two directions. Zone-folded replicas of a parent band can overlap and hybridize with the parent band on a meV energy scale. In contrast, parent and zone-folded replica bands in a bulk crystal overlap on an eV scale. In a one-dimensional superlattice, zone-folding occurs on a meV energy scale but does not create replica bands. As a result of the more complicated zone folding in a two-dimensional array, greater distortion on a meV energy scale of the bands of a two-dimensional array is possible. Band gaps, masses, and widths can be tailored by the choice of nanostructure potential.

The two-dimensional, imposed potential was defined by an array of quantum nanostructures. Three choices for the quantum nanostructure were tested. Isolated quantum boxes contain bound states. When quantum boxes are placed in a two-dimensional, periodic array, the band structure still possesses low-energy quasibound states. The number of states and the dispersion are controlled by the size and depth of the well and by the lattice constants. Enhanced optoelectronic properties are predicted for isolated quantum boxes because these structures confine carriers in all dimensions. Quasibound states will still exist when boxes are coupled in an array. Thus arrays of quantum boxes should possess the enhanced optoelectronic properties of isolated boxes modified by the interbox coupling possible in an array.

Extended two-dimensional quantum barriers are used to confine electrons in quantum wells. Quantum bumps, which are barriers with finite spatial extent, also effectively exclude carriers from the barrier regions. When quantum bumps are placed in a two-dimensional array, channels are formed. Low-energy electrons localize at the connections between channels and form bonds between the connections. The dispersion of these states is determined by the width of the channels. The connections become quantum boxes if adjacent bumps touch and block off the channels.

The band structures for arrays of quantum resonators have also been calculated. States which exist in the channels between resonators, and resonance states sensitive to the size of the resonator core, can both exist. The energies and dispersion of these states can be controlled by the choice of the inner and outer resonator radius and the channel width. Structures can be designed so that channeling and resonance states overlap in energy and strongly hybridize.

Two-dimensional arrays of quantum nanostructures could be used to tailor the electronic properties—band masses, gaps, and widths—of a two-dimensional electron system. Moreover, the choice of nanostructure determines the type of states in the band structure. The states can be tailored to be free states, quasibound states, channeling states, or resonance states. The full range of lattice geometries, types of nanostructures, and unit-cell configurations still must be explored to determine the range of electronic properties that could be tailored.

ACKNOWLEDGMENTS

This research was conducted under the McDonnell Douglas Independent Research and Development Program. Collaboration with D. B. Murray and A. H. MacDonald during the preliminary phase of this work is greatly appreciated.

[1]For some examples, see U. Mackens, D. Heitman, L. Prager, J. P. Kotthaus, and W. Beinvogl, Phys. Rev. Lett. **53**, 1485 (1984); D. Heitman, J. P. Kotthaus, U. Mackens, and W. Beinvogl, Superlatt. Microstruct. **1**, 35 (1985); J. P. Kotthaus, in *Interfaces, Quantum Wells, and Superlattices,* edited by C. R. Leavens and R. Taylor (Plenum, New York, 1988), p. 95; W. Hansen, M. Horst, J. P. Kotthaus, U. Merkt, C. Sikorski, and K. Ploog, Phys. Rev. Lett. **58**, 2586 (1987); M. J. Kelly, J. Phys. C **18**, 6341 (1985); W.-M. Que and G. Kirczenow, Phys. Rev. B **37**, 7153 (1988).

[2]For some examples of arrays of isolated quantum boxes, see S. J. Allen, Jr., H. L. Störmer, and J. C. M. Hwang, Phys. Rev. B **28**, 4875 (1983); M. A. Reed, R. T. Bate, K. Bradshaw, W. M. Duncan, W. R. Frensley, J. W. Lee, and H. D. Shih, J. Vac. Sci. Technol. B **4**, 358 (1986); K. Kash, A. Scherer, J. M. Worlock, H. G. Craighead, and M. C. Tamargo, Appl. Phys. Lett. **49**, 1043 (1986); H. Temkin, G. J. Dolan, M. B. Panish, and S. N. G. Chu, Appl. Phys. Lett. **50**, 413 (1987); Y. Miyamoto, M. Cao, Y. Shingai, K. Furuya, Y. Suematsu, K. G. Ravikumar, and S. Arai, Jpn. J. Appl. Phys. **26**, L225 (1987).

[3]For some examples of arrays of quantum boxes which could or do couple, see G. Bernstein and D. K. Ferry, Superlatt. Microstruct. **2**, 373 (1986); J. Cibert, P. M. Petroff, G. J. Dolan, S. J. Pearton, A. C. Gossard, and J. H. English, Appl. Phys. Lett. **49**, 1275 (1986); P. M. Petroff, J. Cibert, A. C. Gossard, G. J. Dolan, and C. W. Tu, J. Vac. Sci. Technol. B **5**, 1204 (1987); K. Kash, J. M. Worlock, M. D. Sturge, P. Grabbe, J. P. Harbison, A. Scherer, and P. S. D. Lin, Appl. Phys. Lett. **53**, 782 (1988).

[4]D. K. Ferry, Phys. Status Solidi B **106**, 63 (1981).

[5]G. J. Iafrate, D. K. Ferry, and R. K. Reich, Surf. Sci. **113**, 485 (1982).

[6]G. J. Iafrate, in *The Physics of Submicron Structures,* edited by H. L. Grubin, K. Hess, G. J. Iafrate, and D. K. Ferry (Plenum, New York, 1984), p. 301.

[7]R. K. Reich, R. O. Grondin, and D. K. Ferry, Phys. Rev. B **27**, 3483 (1983).

[8]A. E. Carlsson and N. W. Ashcroft, Phys. Rev. B **29**, 6791 (1984).

[9]W.-M. Que and G. Kirczenow, Phys. Rev. B **38**, 3614 (1988).

[10]A preliminary report of this work is part of G. W. Bryant, D. B. Murray, and A. H. MacDonald, Superlatt. Microstruct. **3**, 211 (1987).

[11]T. L. Loucks, *Augmented Plane Wave Method* (Benjamin, New York, 1967).